X-ray diffraction from rectangular slits

D. Le Bolloc'h,[a] F. Livet,[b]* F. Bley,[b] T. Schulli,[c] M. Veron[b] and T. H. Metzger[c]

[a]LPS, UMR-CNRS8502, U. Paris-Sud, Bat. 510, 91405 Orsay CEDEX, France, [b]LTPCM-ENSEEG, UMR-CNRS5614, INPG/UJF BP 75, 38402 St Martin d'Heres, France, and [c]European Synchrotron Radiation Facility, BP 220, 38043 Grenoble CEDEX, France. E-mail: flivet@ltpcm.inpg.fr

It is shown that for micrometre-sized beams the X-ray diffraction from slits is a source of strong parasitic background, even for slits of high quality. In order to illustrate this effect, the coherent diffraction from rectangular slits has been studied in detail. A large number of interference fringes with strong visibility have been observed using a single set of slits made of polished cylinders. For very small apertures, asymmetrical slits generate asymmetrical patterns. This pattern is calculated from the theory of electromagnetic field propagation and compared with experiment in the far-field regime. The use of guard slits to remove Fraunhofer diffraction from the beam-defining slits is treated theoretically. Numerical simulations yield the optimum aperture of the guard slits with respect to the distance to the primary slits. Diffraction theory is shown to be essential to understand how to reduce the background-to-signal ratio in high-resolution experiments.

Keywords: X-ray diffraction; slits; small-angle scattering.

1. Introduction

The high brilliance of third-generation synchrotron radiation sources favours the use of small beam sizes, extending below 10 μm, while maintaining a reasonable intensity. This is of great interest for probing micrometer-sized objects, for diffraction at very small angles (Ehrburger-Dolle *et al.*, 2001) or for speckle and coherent scattering experiments (Geissler *et al.*, 2000; Livet *et al.*, 2001). To obtain well defined beams, however, is a challenging task. The first simple experimental limitations are those due to diffraction, which can be expressed approximately in terms of the beam divergence (FWHM) ϵ and the beam size φ,

$$\epsilon\varphi \geq \lambda/2. \qquad (1)$$

In practical experiments, imperfections of the optics make it necessary to use slits (or pinholes), either to limit the beam size or to reduce background scattering ('guard slits'). However, in addition to loss of intensity, slits can generate adverse effects that reduce resolution and prevent measurements close to the direct beam.

As an example, Fig. 1 shows the diffraction from slits consisting of tungsten blades closed to 2 μm × 2 μm. In this experiment the beam was coherent, which means that the equality in relation (1) applied. For such small apertures the surface state of the blades is important. When the aperture size has the same scale as the surface roughness, intense irregular parasitic streaks are observed. In Fig. 1, images obtained by scanning electron microscopy (SEM) reveal scratches due to the grinding of the surface of the slits.

In this paper we analyse the use of slits in high-resolution experiments as well as the intrinsic background from slit diffraction. In order to limit scattering such as in Fig. 1, carefully polished blades of cylindrical shape have been used. In the first part of this article we discuss this choice and the results that were obtained with a set of slits of high accuracy. Measured diffraction fringes are compared with calculations based on electromagnetic wave propagation theory.

To obtain a well defined narrow beam such as is necessary in X-ray small-angle scattering (SAXS) experiments, guard slits are used to remove the fringes and diffraction effects from the first slits and to limit the background. In the second part of this article the fundamental parasitic scattering from slits and the combined effect of a set of two slits is calculated. We show that background is essentially a diffraction effect, which can be calculated to optimize the experimental arrangement.

All experiments described in this paper were carried out on the ID01 beamline at the ESRF. This beamline has polished Be windows which can be removed from the beam.

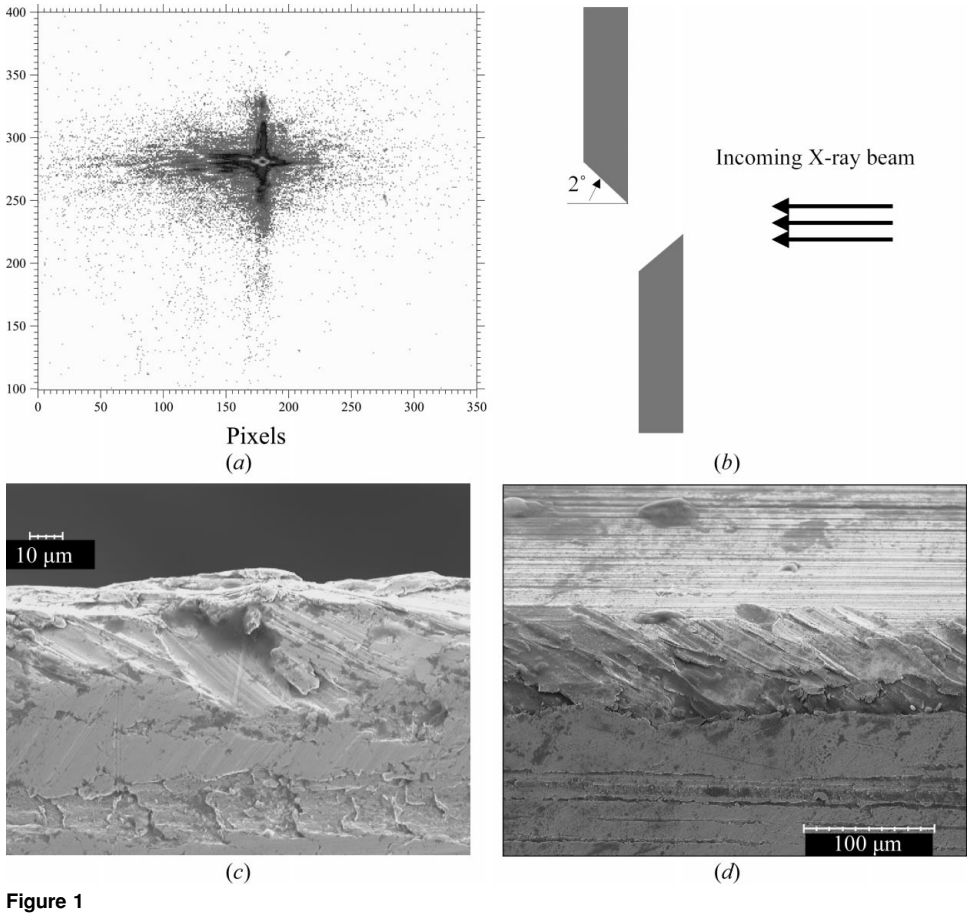

Figure 1
(*a*) Diffraction from a single set of 2 mm-thick tungsten blade slits. The aperture is reduced to 2 μm × 2 μm (E = 8 keV; slit–CCD camera distance = 1.75 m, pixel size = 22 μm). The beam is essentially coherent. Irregular streaks can be seen. (*b*) Blade configuration. SEM images of profile (*c*) and front view (*d*) of the edge of a tungsten blade.

2. Diffraction from polished slits

2.1. Cylindrical edges

In Fig. 1 the irregular scattering is due to two reasons. The first one relates to surface roughness and inhomogeneity of sintered tungsten blades which hardly surrender the polishing procedures. The second reason is the X-ray scattering from the sharp blade edges. The geometry of cylindrical edges is sketched in Fig. 2. Let α_c be the critical angle for total reflection. If an X-ray strikes the second cylinder with an angle of incidence α, then (i) either $\alpha < \alpha_c$, and the X-ray is reflected at an angle 2α, or (ii) $\alpha > \alpha_c$, and it is absorbed, provided that $\mu^{-1} << 2R\alpha_c$.

For molybdenum at 8 keV, $\alpha_c = 0.44^\circ$, and $\mu^{-1} = 6.44$ µm. For $R =$ 1 mm, $2R\alpha_c = 16$ µm. Transmission of X-rays can be neglected here but, for higher X-ray energies, tantalum slits are necessary.

Cylinders of a hard metal like Mo can be easily polished with diamond powder to a state of high surface quality. The absence of sharp edges effectively removes parasitic scattering. In this situation the surface acts as a mirror for case (i). The part of the incident beam involved in this reflection corresponds to a width of about

$$0.5R\alpha_c^2 \simeq 0.03\ \mu\text{m} \qquad (2)$$

at each cylinder edge. This is a small fraction of a few µm beam size. The average reflecting angle is large (about half a degree) and guard slits can conveniently remove this contribution to the background.

Cylinders were mounted on high-precision slits, with a reproducibility of about 0.2 µm. The mechanical design of these slits was developed at the ESRF.

The diffraction pattern of a single set of slits consisting of four molybdenum cylinders with an aperture of 2 µm × 2 µm is displayed in Fig. 3. The incoming beam was limited by primary slits to 200 µm × 200 µm at 10 m, just after the optics of the ID01 beamline of the ESRF. Under these conditions, in the absence of perturbation, the beam can be considered as a fully coherent plane wave. This measurement was performed at $E = 8$ keV with the detector located 1.75 m from the slits. A direct-illumination CCD camera was used on account of its high resolution (22 µm), and the 'droplet algorithm' (Livet *et al.*, 2000) ensured low noise and large dynamic range for X-ray registration. The first pattern (Fig. 3*a*) was obtained in air, with Al attenuators to protect the CCD camera from the direct beam. To reduce the background, the same measurement was performed completely under vacuum with no attenuator or Be window (Fig. 3*b*). A 0.5 mm-diameter beamstop was used to protect the CCD camera.

Both figures display asymmetric diffraction patterns with a large number of interference fringes. The contrast (visibility) between fringes is strong and diagonal fringes are visible. On the right-hand side of Fig. 3, the period of the horizontal fringes decreases with increasing distance from the central peak. This asymmetry is due to the asymmetry of the slit (Vlieg *et al.*, 1997; Libbert *et al.*, 1997). The analytical expression of this asymmetric profile is given in the following section.

2.2. Coherent diffraction of a single slope slit

Diffraction of a plane wave by a single rectangular aperture is well known (Born & Wolf, 1980) and can be solved analytically in the far-field regime (Fraunhofer approximation). The near-field/far-field boundary Λ is here defined by

$$\Lambda \simeq \varphi^2/\lambda, \qquad (3)$$

where φ is again the beam size.

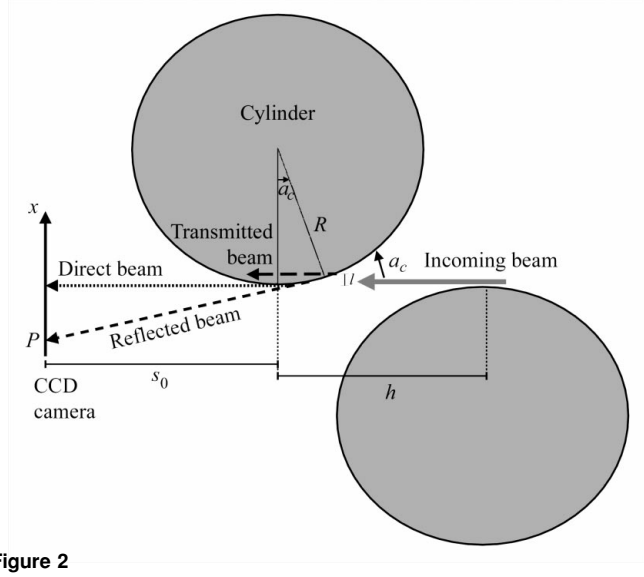

Figure 2
Sketch of two cylinders (dimensions not to scale). Some intensity is reflected by the cylinder surface for $\alpha < \alpha_c$. If $\alpha > \alpha_c$, X-rays are strongly absorbed.

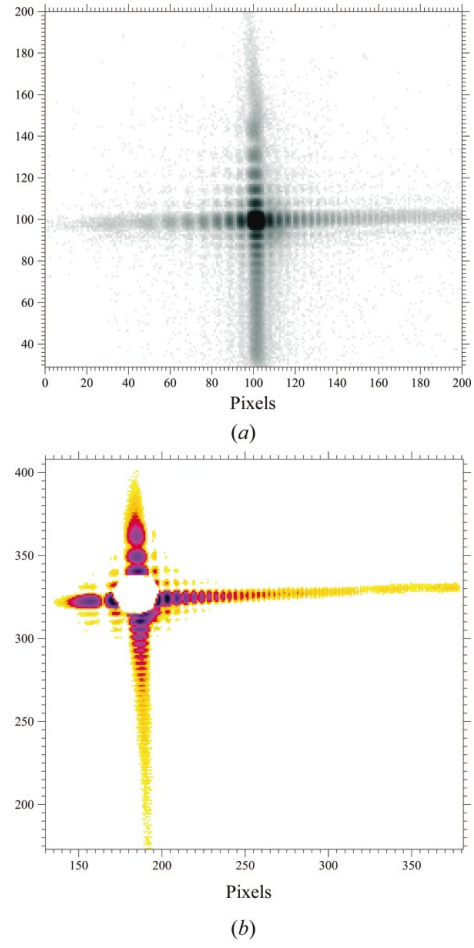

Figure 3
(*a*) Diffraction pattern from the cylindrical slit system. The cylinders were polished with 1/4 µm diamond paste. (*b*) Same diffraction pattern in completely evacuated surroundings, without attenuators or Be window. A 0.5 mm-diameter beamstop was used to protect the CCD from the direct beam. Strong asymmetry is visible. These patterns were recorded at 1.75 m from the slit ($E = 8$ keV).

A sketch of the slits configuration is shown in Fig. 4. A 3 mm distance between opposite cylinders means that some modifications to the coplanar slits calculation of Born & Wolf (1980) are required. Using the same notations as Born & Wolf (1980), the scattered amplitude at the point $P(x,y)$ on the detector coming from a rectangular aperture of sides $2a$ and $2b$ can be written as

$$A(P) = C \iint \exp[ik(r+s)]\, \mathrm{d}\zeta \mathrm{d}\eta, \tag{4}$$

where $r = ||\vec{OM}||$ is the distance between the source O and a point $M(\zeta, \eta)$ of the aperture, and $s = ||\vec{MP}||$, where P is a point on the detector.

This integral can be calculated by expanding the optical path $(r+s)$ as a function of ζ and η.

It can be assumed that the line between the slit edges is almost horizontal, with an inclination α. The optical path $r+s$ decomposes into

$$r = \left[(\zeta \sin\alpha)^2 + \eta^2 + (r_o + \zeta\cos\alpha)^2\right]^{1/2},$$
$$s = \left[(x - \zeta \sin\alpha)^2 + \eta^2 + (s_o - \zeta\cos\alpha)^2\right]^{1/2},$$

where s_o and r_o are the source–slit and slit–detector distances, respectively. Despite the fact that, in the previous equation, $\zeta_{\max} \simeq h/2 = 1.5$ mm is much larger than in the symmetric case, the distance above which the second-order terms in ζ and η can be neglected is the same as in the symmetric case: the near-field/far-field distance is $\Lambda \simeq 3$ cm for $\varphi \simeq 2$ µm, much smaller than s_o ($\simeq 1.75$ m) and r_o ($\simeq 10$ m).

It can be shown that the first-order terms can be written

$$\begin{aligned} s &= s_o - \zeta\left[(x/s_o)\sin\alpha + \cos\alpha\right]\left[1 - \tfrac{1}{2}(x/s_o)^2 + \tfrac{3}{8}(x/s_o)^4 + \ldots\right] \\ &= s_o - \zeta\left[(x/s_o)\sin\alpha + \cos\alpha\right]\left[1 + (x/s_o)^2\right]^{-1/2} \\ &= s_o - \zeta(\sin\alpha\sin\beta + \cos\alpha\cos\beta) \\ &= s_o - \zeta\cos(\alpha - \beta) \end{aligned} \tag{5}$$

and

$$r = r_o + \zeta\cos\alpha,$$

with $\tan\beta = x/s_o$. The asymmetric intensity is deduced,

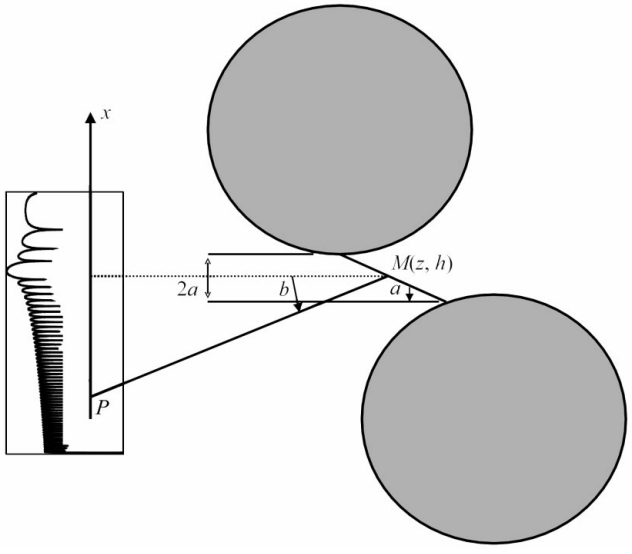

Figure 4
Sketch of asymmetrical slits (not to scale). For $x > 0$, the aperture appears smaller than for $x < 0$, giving rise to more widely spaced fringes.

$$I(P) \propto (hb)^2\left[\frac{\sin(kwh/2)}{kwh/2}\right]^2\left[\frac{\sin(kyb/s_o)}{kyb/s_o}\right]^2, \tag{6}$$

with

$$w = \cos\alpha - \cos(\alpha - \beta). \tag{7}$$

To first order,

$$wh/2 \simeq -\frac{x}{s_o}\left(a - \frac{xh}{4s_0}\right). \tag{8}$$

Now, the effective aperture $a' = a - (xh/4s_o)$ depends on the position x on the detector. For $x > 0$ then $a' < a$ and the fringes appear more widely spaced. For $x < 0$ ($a' > a$) the fringes appear closer (see Fig. 4).

2.3. Computer calculation of slit scattering

Analytic calculations compare well with the experiment (see Fig. 5), but they are restricted by simple situations. In order to obtain results in more complex experimental set-ups, we performed computer simulations of the diffracted intensity. To fit experimental conditions, a point source was assumed to lie at a distance of 10 m away from our experimental set-up. As this distance is large, the incoming beam can be considered as a plane wave. In the vicinity of the sample, this wave is limited by slits or pinholes. The wave propagating across the asymmetrical set of slits is calculated in a plane perpendicular to the beam for each slit edge. The wave amplitude $A_0(\vec{r}_0)$ in a plane can be deduced from the wave amplitude $A(\vec{r})$ in a previous plane at a distance D,

$$A_0(\vec{r}_0) = (ik/2\pi D)\int A(\vec{r}) \exp ik(|\vec{r} - \vec{r}_0|)\, \mathrm{d}^2 r. \tag{9}$$

This equation corresponds to the Huygens–Fresnel principle (Born & Wolf, 1980; §8.2). Amplitudes are integrated in a 'nearly semi-infinite' plane, limited on one side by the edge of the slit. Limits in other directions are chosen large enough, and the integration step is chosen small enough so that oscillations due to cut-off and to finite integration steps become negligible. All these choices correspond to Nyquist sampling theorem considerations.

This means that four successive surface integrals are calculated for the estimate of wave amplitudes across asymmetrical slits. Corresponding intensities in the detector yield satisfactory agreement with experiment, as shown in Fig. 6.

In this figure, simulated results are scaled to equalize the maximum intensities (33000 counts in the central pixel) and to set the lower level equal to unity. Vertical scales are logarithmic and the diffraction is plotted only for the central square of the CCD detector of side 50 pixels. The simulations assumed a 2 µm × 2 µm square aperture, and, apart from experimental Poisson noise, the main discrepancy between simulation and experiment can be attributed to an underestimate of the slit aperture: a value of 2.2 µm yields a better fit, as observed in Fig. 5.

3. Slit scattering and experimental SAXS set-up

3.1. Wide-angle parasitic scattering from slits

In the situation where the beam is coherent and the resolution of the detector is sufficiently good, beautiful oscillating intensities can be observed, as in Fig. 6. These were obtained with a slit aperture $d_1 = 200$ µm after the ID01 optics hutch at a distance $D_1 = 10$ m before the experimental set-up. A square slit aperture $\varphi = 2$ µm was placed close to the goniometer centre and the slit-to-detector distance was $D_2 = 1.75$ m. It can be shown that the coherence properties of the experiment depend on a dimensionless ratio z

(Livet *et al.*, 1998), the value of which is $z_1 = \pi\varphi d_1/2\lambda D_1 \simeq 0.4$ for the beam and $z_2 = \pi\varphi d_2/2\lambda D_2 \times 0.3$ for the detector. Low values of z provide good conditions for the observation of interference effects. As these two ratios are significantly smaller than unity, the quality of the resulting Fraunhofer fringes is excellent (see Fig. 6).

The oscillations discussed earlier in this paper correspond to strong 'wide'-angle scattering. This parasitic scattering is the consequence of slit diffraction, and is not limited to the case of coherent beams. This can be seen from Fig. 7, where the scattering is measured for various apertures of the slits. In all cases, streaks are observed although, for $\varphi \geq 5$ µm, coherence is poor and no significant oscillations are observed by the detector. The circularly averaged wide-angle scattering of the slits can be estimated. If the intensity is normalized [$I(q = 0) = 1$], the q dependence of I can be expressed as

$$I(q) = (2\pi/S) \int J_0(q\rho)\gamma(\rho)\rho \, \mathrm{d}\rho, \tag{10}$$

where J_0 is a Bessel function and S is the area of the aperture. The isotropically averaged Patterson function $\gamma(\rho)$ can be written to first order in terms of the total length l (= 4φ) of the slit edges,

$$\gamma(\rho) \simeq 1 - (l\rho/\pi S). \tag{11}$$

The isotropically averaged asymptotic intensity is then

$$I(q) = 2l/q^3S^2. \tag{12}$$

This latter can be compared with the total intensity crossing the slits,

$$\int I(q)\,\mathrm{d}^2q = 4\pi^2/S. \tag{13}$$

This asymptotic behaviour can be observed from a plot of $I(q)q^3$, as shown in Fig. 8.

Table 1 lists the values of N_0 (maximum number of counts), $\int I(q)\,\mathrm{d}^2q$ and $\lim_{q=\infty} q^3I(q)$, normalized by the estimate of N_0, as in equations (13) and (12).

For the measurements of Fig. 7, to normalize $I(q)$, a precise estimate of N_0 is required. This is difficult to obtain here for $\varphi > 5$ µm, because the detector resolution is low.

For this reason, the ratio

$$\frac{4S}{l} = \frac{2\int I(q)\,\mathrm{d}^2q}{\pi^2 \lim_{q=\infty} q^3I(q)} \tag{14}$$

was estimated (last column of Table 1). This should be equal to φ, and does not depend on the estimate of N_0.

In the q range discussed here ($q < 0.5 \times 10^{-3}$ Å^{-1}), the majority of the overall experimental background signal can be attributed to the length l of the slit edges. The ratio in equation (14) only compares the total beam intensity with the asymptotic behaviour. It does not depend on detector resolution, and the beam needs not necessarily to be fully coherent. It is an intrinsic experimental feature. In the measurement of Fig. 7, scattering from air remains negligible, and the observed background is explained by the cut-off introduced by the slits.

In the case of unpolished slits, like in Fig. 1, edge imperfections can increase the background. However, the main effect is probably 'erratic scattering', and the directional intensity, perpendicular to the straight edges, measured in Fig. 8 is spread among various directions. Increase of the angular average background can occur mainly if l in equations (11)–(14) increases due to surface roughness. As these results are also valid if the beam is not coherent, equation (14) places a lower bound on the scattering from slits when used for beam definition. Here, it is assumed that the incoming beam is homogeneous, which is obviously not the case if the slits are used as guard slits.

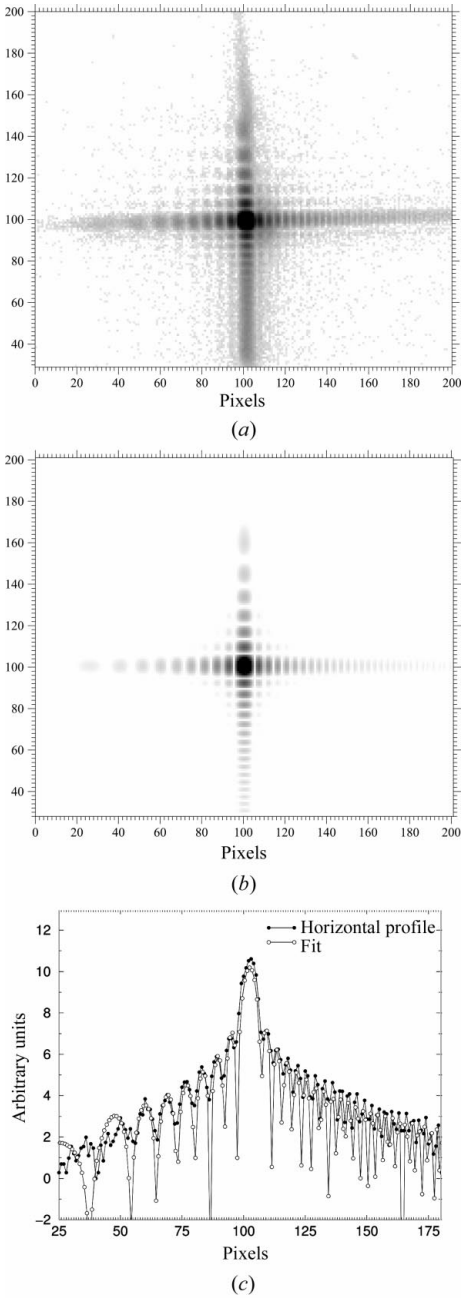

Figure 5
Comparison between (*a*) experimental diffraction pattern (corresponding to Fig. 3) and (*b*) fit using equation (6). The fit indicates an aperture of 2.49 µm (H) × 2.28 µm (V). (*c*) Fit along the horizontal profile (log units).

Table 1
Estimates of the total peak intensity, the normalized integral (equation 13), the asymptotic behaviour (equation 12) and the ratio (equation 14) for various slit apertures.

Slit aperture (µm)	N_0	$\int I(q)\,\mathrm{d}^2q$	$\lim_{q=\infty} q^3I(q)/I(q=0)$	φ estimated (µm)
10	33500	1.275×10^{-8}	1.8×10^{-14}	14
7	29600	1.365×10^{-8}	3.0×10^{-14}	9
5	31200	2.07×10^{-8}	8.0×10^{-14}	5.
3	35800	3.88×10^{-8}	3.0×10^{-13}	2.7
2	32700	7.15×10^{-8}	7.0×10^{-13}	2.1

3.2. Background and guard slits

The results discussed in the first part of this paper correspond to experiments where the beam is fully coherent, and the calculation of slit diffraction assumes plane waves crossing the aperture. In this case the source is considered as a point source.

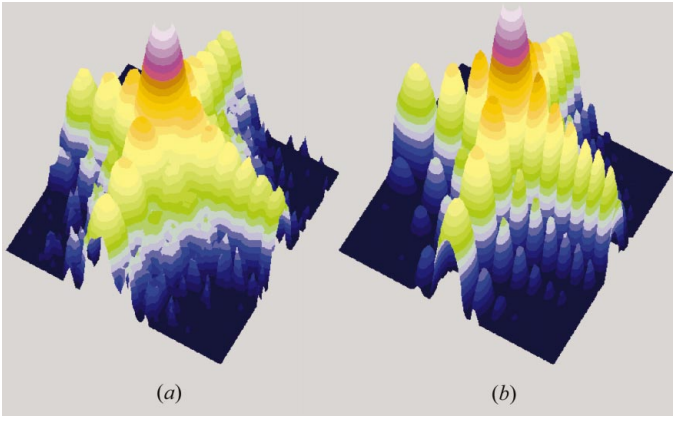

Figure 6
Measured (*a*) and simulated (*b*) scattering from 2 μm asymmetric slits.

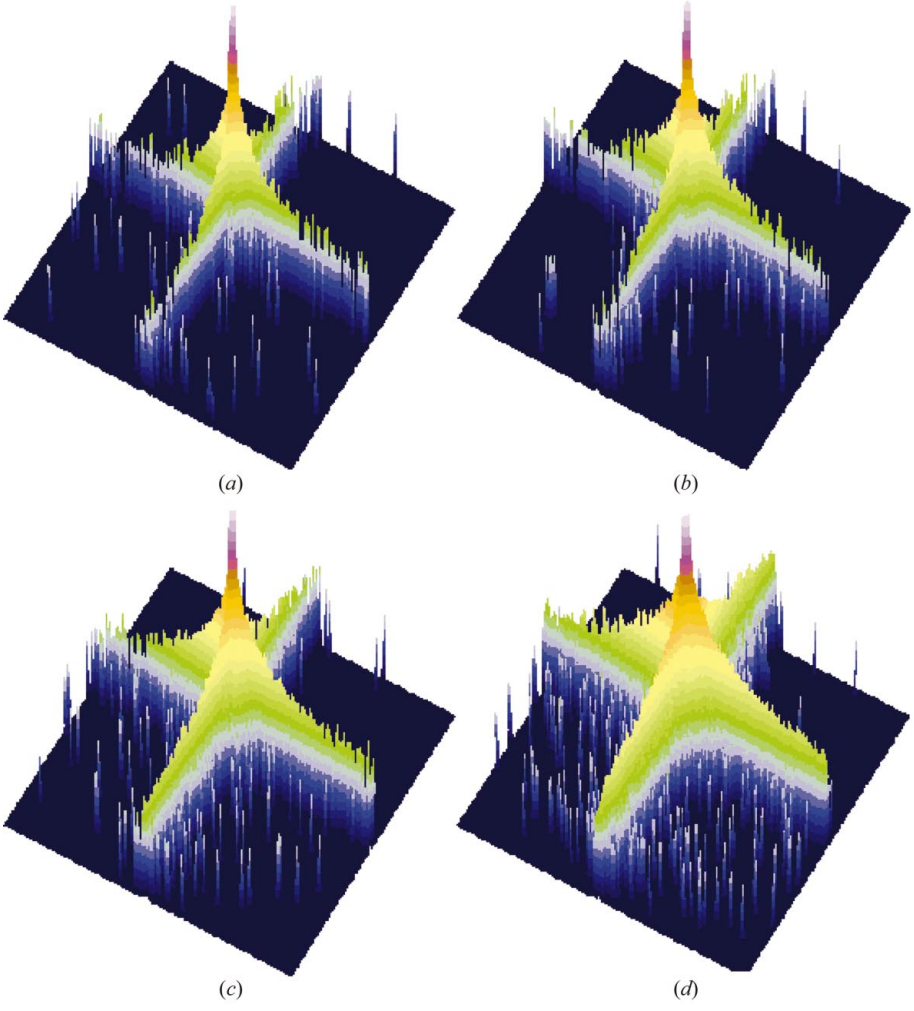

Figure 7
Scattering from square asymmetrical slits. Apertures are (*a*) 10 μm, (*b*) 7 μm, (*c*) 5 μm and (*d*) 3 μm, detector at 1.75 m, 200 × 200 pixels of size 22 μm.

In the case of a coherent beam, small-angle X-ray scattering (SAXS) experiments require reduced parasitic scattering in the measured range of the q vector. This is achieved by inserting guard slits between pinhole and sample (Livet *et al.*, 2001; Geissler *et al.*, 2000), which causes a distortion of the shape of the wave after the pinhole. It seems obvious that the guard slit configuration must be intermediate between the two simple limiting cases:

(i) if the guard slits are closed to the same size as the pinhole aperture, they generate strong diffraction, equivalent to that of the pinhole alone;

(ii) if the guard slits are opened wide they do not reduce significantly the small-angle diffraction from the pinhole.

Moreover, the relative positions of the pinhole (or defining slits), guard slits and sample are important parameters in the experimental set-up.

These parameters can be used to estimate the feasibility of SAXS measurements in the very low q region, *i.e.* having a background sufficiently low to use area detectors and an efficient beamstop. For this aspect, the relevant distance between pinhole and guard slits is Λ in equation (3).

In a practical synchrotron experiment, if the pinhole-to-sample distance is significantly larger than Λ, the effective beam size is increased at the sample. This causes a contraction of the speckle structure, making it difficult to observe. On the other hand, to achieve optimum background reduction, the guard slits must be sufficiently far from the pinhole. Fulfilling these conditions leads to a sample position as close as possible to the guard slits. For this reason, the discussion is limited to two parameters in the vicinity of the sample: the aperture d of the guard slits and the distance D between aperture and guard slits. The dependence of the background intensity on angle was estimated in a standard configuration used for coherent SAXS measurements, with a pinhole–detector distance of 2.9 m and where, as previously, the pinhole consists of slits closed to 10 μm.

Fig. 9 shows typical results (D = 0.4 m) of the calculations. These were obtained in the horizontal direction, where the background intensity is maximum (see Fig. 7). The top curve corresponds to the normal Fraunhofer slit pattern, and the effect of guard slits can be appreciated from the two other curves. For a guard slit aperture of 24 μm, a rapid decrease in intensity is found, with the background decreasing by two orders of magnitude for $q > 2.5 \times 10^{-4}$ Å^{-1}, after which it runs parallel to the diffraction from the single 10 μm slit. For the 48 μm guard slit, the background decreases by a further factor of three, but only from $q > 5 \times 10^{-4}$ Å^{-1}.

The normalized two-dimensional background intensity can, to a very good approximation, be written as

$$I(q_x, q_y) = I(q_x, q_y = 0)I(q_x = 0, q_y). \quad (15)$$

In a 'diagonal' direction of the area detector, the decrease in intensity is much faster. For $Q = (q_x, q_x)$, *i.e.* $|Q| = q_x 2^{1/2}$, the decrease must be squared and parasitic intensity can be reduced by four to five orders of magnitude in these examples, for either $q > 3.5 \times 10^{-4}$ Å^{-1} or $q > 7 \times 10^{-4}$ Å^{-1}.

The asymptotic directional behaviour of the background scattering of this set-up can be estimated, assuming that the guard slits are in a far-field position. For $q_y = 0$ (as in Fig. 9), we find

$$I(q_x, q_y = 0) \simeq \frac{4}{\pi^2}\left(\frac{\lambda D}{\varphi d}\right)^2 \left[\sin\left(\frac{\pi d \varphi}{\lambda D}\right)\right]^2 \left[\frac{\sin(q_x d/2)}{q_x \varphi/2}\right]^2. \qquad (16)$$

This equation compares well with the results of Fig. 9: the fast oscillatory factor has a q_x^{-2} behaviour at large q, similar to that calculated without guard slits, and the oscillations correspond to diffraction from the guard slits: their period is significantly shorter because the apertures (24 µm and 48 µm) are much larger. Obviously, such oscillations cannot be observed because the resolution of our CCD is too low, and a finite source dimension will further damp them. For the same reason, in practice, $[\sin(\pi d\varphi/\lambda D)]^2$ can be replaced by 0.5. The main result of equation (16) is that the scattering from the 10 µm slit is reduced by a factor $(2/\pi^2)(\lambda D/\varphi d)^2$, *i.e.* 1.4×10^{-2} and 3.6×10^{-3}, respectively, in the cases illustrated in Fig. 9. These values are in good agreement with the numerical results.

Although equation (16) initially assumes a relatively large distance, $D > \Lambda = \varphi^2/\lambda$, it provides a good estimate for the background at 'large' angles ($2\theta > 10^{-4}$ rad) provided that $D \simeq \Lambda$ (here, $D = 0.4$ m and $\Lambda = 0.6$ m). As equation (15) still holds, it is obvious that the introduction of a second set of slits after those limiting the beam increases the relative contrast between the horizontal or vertical directions and the 'diagonal' directions: a factor of 10 reduction in the horizontal direction can give a factor of 100 in the diagonal direction.

Experiments with a coherent beam can be considered as a limiting case in a high-resolution experiment. Conversely, the diffraction calculation can easily be extended to the case of beams of low coherence. This can be found from the above calculations with an extended source.

Results of Fig. 10 were obtained with an extended incoherent secondary source of size 300 µm × 300 µm at 10 m, and can be compared with Fig. 9, where a point source was assumed. Neglecting oscillations, the two figures are similar. This shows that to estimate background in high-resolution experiments, diffraction effects must be taken into account. This is indeed observed on the ESRF BM2 beamline: after the slits are carefully polished, the background has the shape of a cross, even in incoherent experiments. Provided other background sources (windows *etc.*) are low enough, the background becomes strongly anisotropic.

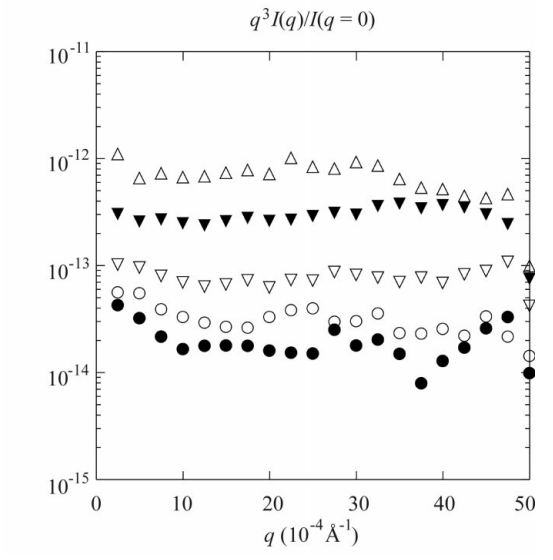

Figure 8
Asymptotic behaviour observed from slits of various sizes (isotropic average). From bottom to top: 10 µm, 7 µm, 5 µm, 3 µm and 2 µm.

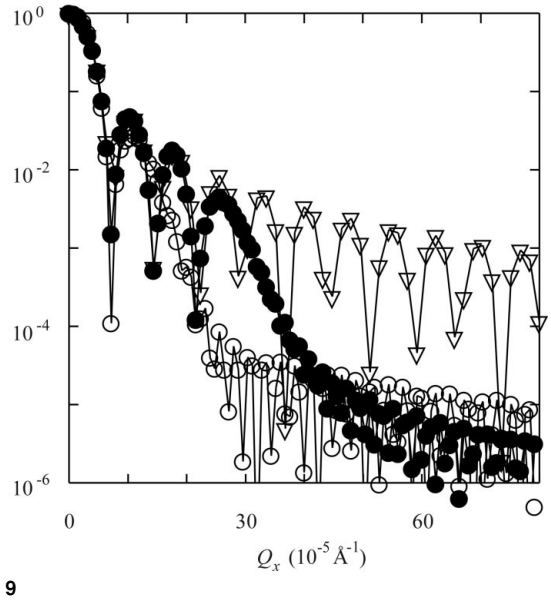

Figure 9
Intensities from a 10 µm aperture pinhole and guard slit apertures of ∞ (triangles), 24 µm (open circles) and 48 µm (filled circles) with $D = 0.4$ m, calculated in the detection plane 2.5 m after the guard slits.

3.3. Beamstop

In SAXS experiments, measurements at very low q values (USAXS) are difficult with area detectors. The main reason is the strong increase of intensity observed, which saturates the electronics,

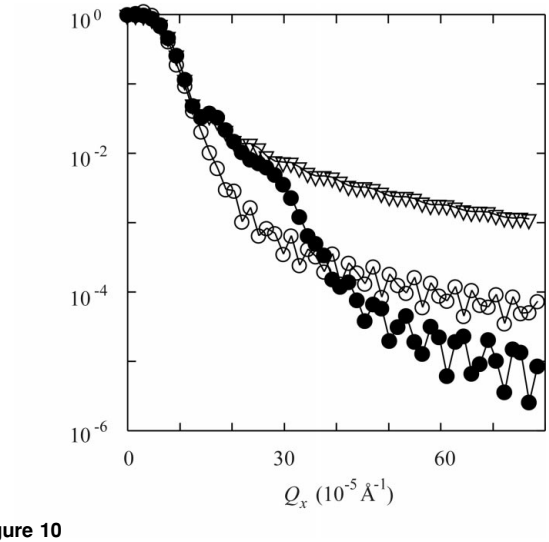

Figure 10
Intensities from a 10 µm aperture and guard slits with apertures of ∞ (triangles), 24 µm (open circles) and 52 µm (filled circles) with $D = 0.4$ m, calculated in the detection plane at 2.5 m after the guard slits. The source is assumed to be 300 µm × 300 µm at 10 m.

and which can even destroy the detector. Usually, background intensity is considered in terms of experimental imperfections. Our results, as seen in Figs. 9 and 10, show that background is intrinsic and corresponds to diffraction from the optical elements.

In the case where the slits are carefully polished and aligned, the scattering can be calculated from first principles. The more general case of an incoherent beam can be modelled by the superposition of intensities from all points of an incoherent extended source.

The shape of the scattering pattern from slits is strongly anisotropic and this anisotropy increases when guard slits are added, even if total parasitic scattering is reduced. This suggests a new shape for beamstops. In Fig. 11 the parasitic SAXS scattering is shown as a function of guard slit aperture for configurations similar to those of Fig. 9. All background intensities are normalized by the total intensity crossing the first set of slits. A 1 mm square detector is assumed to be located at a distance of 2.5 m from the guard slits, as in Figs. 9 and 10. The intensity, shown as a function of guard slit aperture d, is the parasitic scattering integrated over this small detection area, after elimination of pixels corresponding to two different beamstops: a circular beamstop of diameter 0.5 mm and a cross-shaped beamstop, which can be idealized as two wires, one horizontal and one vertical, crossing at the centre of the beam, of diameter 400 μm.

In both cases, the q range of measurement is 0.5–1.0 $\times 10^{-3}$ Å^{-1}.

Two calculations were carried out. (i) In the first case the beam is assumed to be fully coherent, and results similar to those of Fig. 9 (point source at 10 m, square slits of size 10 μm, guard slits of variable sizes at a 0.4 m distance) were summed over the area of the 1 mm × 1 mm detector. (ii) To simulate an incoherent experiment, the same source size as in Fig. 10 (300 μm × 300 μm at 10 m) was assumed.

In case (i), the results are a strongly oscillatory function of d, in which the oscillations arise from the full coherence of the beam. They come from the term $[\sin(\pi d\varphi/\lambda D)]^2$ in equation (16). The oscillations are damped in the case of beams of low coherence. If the oscillations are neglected, the same behaviour is observed in the two cases:

(i) the background is three orders of magnitude lower with the cross-shaped beamstop;

(ii) for large values of d the background increases (the limits for $d = \infty$ are 0.022 for the circular beamstop and 3.0×10^{-4} for the cross-shaped beamstop with a point source);

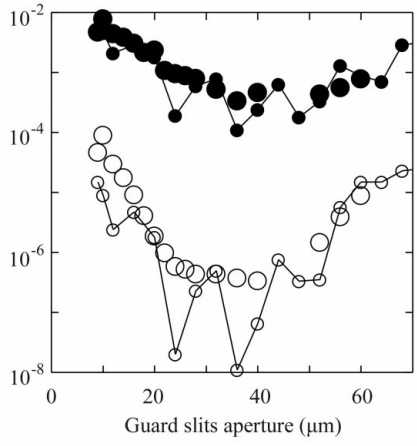

Figure 11
Calculated background intensities received on a 1 mm × 1 mm detector from a 10 μm aperture with guard slits of various apertures d at $D = 0.4$ m. The detection plane is 2.5 m beyond the guard slits. Circular beamstop: filled circles; cross-shaped beamstop: open circles. Results for an extended source (300 μm × 300 μm at 10 m) are also shown (large filled and open circles).

(iii) for small values of d, a rapid increase of the background is observed.

Experimentally, this behaviour is routinely observed. In SAXS experiments, careful adjustment of the guard slits is an important parameter. An initial decrease in background on closing the slits is followed by a rapid increase when the beam 'hits' the slits. The conventional interpretation of this effect is reflection from the surface of the slits. If this were the case, it would be strongly dependent on slit shape and quality. From our results, the increase in background intensity when the beam hits the guard slits is of the order of 0.5% of the beam intensity in the narrow region of detection of Fig. 11, and this is essentially a streak in the direction perpendicular to the slit edges. Such diffraction from slit edges is different from surface scattering, whose contribution for perfectly polished slits of diameter 2 mm corresponds to a negligible fraction of the incoming beam. After the guard slits, the reflected intensity corresponds to an angle $2\theta \simeq 2.0 \times 10^{-4}$ rad $\simeq 2\alpha_c/100$. This angle θ must replace α_c in equation (2), and, correspondingly, only a few angströms of the incident beam width will contribute to the background.

According to our calculations, on average, the increase of the background intensity weakly depends on the detailed shape of the slits, and is essentially due to diffraction phenomena. This background is irregularly scattered in the case of unpolished blades (like in Fig. 1); the average scattering remains of the same order of magnitude (see equation 12).

4. Conclusion

We have shown that, with carefully polished slits, the scattering observed far apart from the beam centre is a fundamental property of the electromagnetic field corresponding to the X-ray photon beam. For the same reason, the background reduction obtained with guard slits is limited. From our results, typical signal-to-noise ratios in an experimental set-up can be approximately predicted. This means that the low-q limits of a USAXS camera can be deduced from basic optical principles.

This provides a method for the improvements in the design of a USAXS instrument, even in the case of an incoherent (*i.e.* classical) experiment. In this case, for high resolution, beams of small cross section are used, not too far removed from the conditions of coherence.

The USAXS region (0.3–3.0 $\times 10^{-3}$ Å^{-1}), corresponding to the domain of light scattering, offers the possibility of investigating relaxation in opaque systems (Livet *et al.*, 2001; Geissler *et al.*, 2000) by X-ray photon correlation spectroscopy.

Using guard slits at a distance of the order of the near-field/far-field limit Λ efficiently limits background in coherent experiments. Guard slits nevertheless accentuate the background anisotropy. The fact that parasitic scattering with carefully polished slits is essentially elongated perpendicular to the edges reveals the potential of cross-shaped beamstops for USAXS experiments with low noise. This is the base of new improvements for the use of area detectors in the USAXS domain.

The authors wish to thank P. Marion and G. Retout for the development of high-precision slits, and R. Taffut and F. Lesimple for technical assistance. Excellent suggestions were given to the authors by E. Geissler.

References

Born, M. & Wolf, E. (1980). *Principles of Optics*, 6th ed. Oxford: Pergamon.

Ehrburger-Dolle, F., Hindermann-Bischoff, M., Livet, F., Bley, F., Rochas, C. & Geissler, E. (2001). *Langmuir*, **17**, 329–343.

Geissler, E., Hecht, A. M., Rochas, C., Bley, F., Livet, F. & Sutton, M. (2000). *Phys. Rev. E*, **62**, 8308.

Libbert, J. L., Pitney, J. A. & Robinson, I. K. (1997). *J. Synchrotron Rad.* **4**, 125–127.

Livet, F., Bley, F., Caudron, R., Geissler, E., Abernathy, D., Detlefs, C., Gruebel, G. & Sutton, M. (2001). *Phys. Rev. E*, **63**, 036108–1.

Livet, F., Bley, F., Létoublon, A., Simon, J. P. & Bérar, J. F. (1998). *J. Synchrotron Rad.* **5**, 1337–1345.

Livet, F., Bley, F., Mainville, J., Sutton, M., Mochrie, S. G. J., Geissler, E., Dolino, G., Abernathy, D. L. & Gruebel, G. (2000). *Nucl. Instrum. Methods*, A**451**, 596.

Vlieg, E., De Vries, S. A., Alvarez, J. & Ferrer, S. (1997). *J. Synchrotron Rad.* **4**, 210–213.

Received 4 October 2001 • Accepted 27 March 2002